Dynamics, multistability, and crisis analysis of a sine-circle nontwist map

Michele Mugnaine[*]

Department of Physics, Federal University of Paraná, 80060-000 Curitiba, PR, Brazil

Matheus Rolim Sales

Graduate Program in Science – Physics, State University of Ponta Grossa, 84030-900 Ponta Grossa, PR, Brazil

José Danilo Szezech, Jr.

Graduate Program in Science – Physics, State University of Ponta Grossa, 84030-900 Ponta Grossa, PR, Brazil
and Department of Mathematics and Statistics, State University of Ponta Grossa, 84030-900 Ponta Grossa, PR, Brazil

Ricardo Luiz Viana

Department of Physics, Federal University of Paraná, 80060-000 Curitiba, PR, Brazil
and Institute of Physics, University of São Paulo, 05508-900 São Paulo, SP, Brazil

We propose a one-dimensional dynamical system, the sine-circle nontwist map, that can be considered a local approximation of the standard nontwist map and an extension of the paradigmatic sine-circle map. The map depends on three parameters, exhibiting a simple mathematical form but with a rich dynamical behavior. We identify periodic, quasiperiodic, and chaotic solutions for different parameter sets with the Lyapunov exponent and Slater's theorem. From the bifurcation analysis, we determine two bifurcation lines, those that depend on just two of the control parameters, for which the bifurcation that occurs is of the saddle-node type. In order to investigate multistability, we analyze the bifurcation diagrams in the two directions of parameter variation and we observe some regions of hysteresis, representing the coexistence of different attractors. We also analyze different multistable scenarios, as single attractor, coexistence of periodic attractors, coexistence of chaotic and periodic attractors, chaotic behavior, and coexistence of different chaotic bands, by the Lyapunov exponent and the analysis of the domain occupied by the solutions. From the parameter spaces constructed, we observe the prevalence of single attractor and only chaotic behavior scenarios. The multistable scenario is, mostly, formed by different periodic attractors. Lastly, we analyze the crisis in chaotic attractors and we identify the interior and the boundary crisis. From our results, the boundary crisis plays a key role for the extinction of multistability.

I. INTRODUCTION

One-dimensional noninvertible maps are the simplest dynamical systems which present different dynamical behaviors, such as periodic, quasiperiodic, and even chaotic motion. The realm of one-dimensional maps is vast, from the modeling of the dynamics of biological populations by the logistic map [1] to the analysis of the behavior of coupled oscillators by the sine-circle map [2,3]. The convenience of studying one-dimensional maps is the simplicity of the system. We have a simpler mathematical model, not computationally costly, in which phenomena presented by it can be also encountered in higher-dimensional systems [2]. It is also easier and simpler to identify and distinguish the periodic, quasiperiodic and chaotic solutions in one-dimensional maps, compared with the effort required to do the same analysis with differential equations [4]. Higher-dimensional systems can have their dynamics reduced to approximately one-dimensional map dynamics, in the limit of strong dissipation [5], and can also represent the dynamics of two-dimensional systems in the Poincaré section. Briefly, one-dimensional maps are an important tool with regard to the dynamics analysis of complex systems, once we can observe and study their dynamical features and expand, in some form, for more complex systems.

The sine-circle map, introduced by Arnold in 1961, is an answer to the problem of two voltages oscillators coupled nonlinearly [6]. The analysis of the sine-circle map allows us to understand the transition to chaos that occurs by the overlap of model locked resonances at the critical scenario, where the map becomes noninvertible [4,7], or by the quasiperiodic route to chaos [8]. A review of the properties of the sine-circle map can be found in Refs. [4,7,9] and references therein. In addition, the sine circle and other circle maps are also seen as a paradigm solution to the angular position of a torus from a two-independent-frequency system in the Poincaré section [9,10]. Two-dimensional maps can be reduced to the sine-circle map, for example, the standard map, also known as the Chirikov-Taylor map [11,12], by the substitution of the action variable in the angle equation [13]

---
[*]mmugnaine@gmail.com

and also its dissipative version, the dissipative standard map (DSM).

Our question now is which map will be obtained if we take a different two-dimensional system as a starting point to construct a one-dimensional map. To answer this question, we follow the construction of the sine-circle map by the manipulation of the standard map as in Ref. [13], with the standard nontwist map, the simplest nontwist two-dimensional system proposed by del Castillo-Negrete and Morrison [14]. With this construction we obtain a one-dimensional map with three control parameters. The one-dimensional map can also be obtained by the manipulation of a twist map perturbed by two harmonics with different frequencies. With this we have two completely different two-dimensional systems, a twist and a nontwist map, that lead to the same circle map.

In this paper we present a circle map and analyze the dynamics of the system, observing the time series and their respective Lyapunov exponents, and the bifurcations that occur when one of the three parameters varies. We investigate the multistability scenario and the crisis that can occur in the map, and we also perform dynamical analysis based on Slater's theorem, a method to identify and distinguish chaotic, periodic, and quasiperiodic orbits based on the recurrence times [15–18]. We also construct the parameter space of the map, where it is possible to identify the types of solution and how all possible solutions are organized by continuously varying two parameters. MacKay and Tresser, and posteriorly Gallas, analyzed and reported the existence of shrimp-shaped domains in such spaces [19–21]. In these structures the dynamics is periodic, and they frequently appear in the parameter space of dissipative systems, such as a four-dimensional Chua model [22], a two-gene model for chemical reactions [23], an impact oscillator [24], and a system of coupled Hénon maps [25], to cite a few.

The paper is organized as follows: In Sec. II we introduce the one-dimensional map and some of its dynamical properties. In Sec. III we present a dynamical analysis, based on the Slater's condition and on bifurcation diagrams, Lyapunov exponents, and an analytical evaluation of the bifurcation points. The multistability scenario and the crisis of chaotic attractors are investigated in Sec. IV. We present our conclusions in the last section.

II. ONE-DIMENSIONAL MAP

The standard map, also known as the Chirikov-Taylor map or the kicked rotator map [26], is defined by

$$I_{n+1} = I_n + \frac{K}{2\pi} \sin(2\pi\theta_n),$$
$$\theta_{n+1} = \theta_n + I_{n+1}, \qquad (1)$$

where the conjugate coordinates θ and I are computed modulo 1, and K is the nonlinearity parameter, which can represent the strength of the perturbation [27]. The standard map is a paradigmatic model widely used to describe the dynamical behavior and the fundamental properties of Hamiltonian systems, such as the transition from regular to chaotic behavior as well as the chaotic behavior itself [2,27,28]. From an applied point of view, the standard map is the mathematical model obtained by the analysis of a kicked rotor, where the variable

I is the angular momentum and θ is the angular position of the rotor [2]. Furthermore, the standard map can also be applied to the analysis of tokamak magnetic fields in highly idealized situations [27], or used as an local approximation to general nonlinear maps [28].

The sine-circle map can be obtained from Eq. (1) by a simple mathematical manipulation: by substituting I_{n+1} into θ_{n+1}, considering $I_n = \Omega$ a constant, and replacing K for $-K$ [equivalent to a trivial change of variable $\theta \to -\theta$ in Eq. (1)], we obtain

$$\theta_{n+1} = \theta_n + \Omega - \frac{K}{2\pi} \sin(2\pi\theta_n), \ \text{mod} \ 1, \qquad (2)$$

the sine-circle map, also called standard circle map [29,30]. The sine-circle map can also be obtained from the dissipative standard map, as stated by Lichtenberg and Lieberman [28] and Bohr *et al.* [10]. The map is also obtained by the analysis of the phase oscillator with a nonweak periodic external forcing [3].

The sine-circle map is a paradigmatic one-dimensional map, widely used to describe the dynamics of a single oscillator of natural frequency Ω coupled to another oscillator of frequency 1, with a coupling of strength K [8,31]. The map has a simple mathematical form, but the dynamics intrinsic to it is far from being simple. The nature of the possible solutions of Eq. (2) depends heavily on the value of K. For $K < 1$, the map is *subcritical*, monotonic, invertible and, consequently, only quasiperiodic, and periodic solutions are possible [2,7,8,28]. For $K > 1$, the map loses its invertibility and monotonicity, being called *supercritical*, and exhibits chaotic trajectories [8,28,31]. The criticality, for the sine-circle map, occurs at $K = 1$, at which the map loses invertibility once it presents an inflection point of slope zero, by a cubic inflection at $x = 0$ [28,32,33]. With this criticality well established, we know exactly where the chaotic behavior is possible ($K > 1$) and for which values of K the only solutions allowed are quasiperiodic and periodic solutions ($K \leqslant 1$). In addition to the information provided by the critical line $K = 1$, the sine-circle map also allows us to understand the transition from a periodic regime to a quasiperiodic behavior by the tangent bifurcation. as the parameter Ω changes [34], the transition to chaos [7,31,33], the universality of scaling laws for maps with cubic inflection [33], and the construction of the devil's staircase by the phase-locking structure [3,7].

Inspired by the construction of the map in Eq. (2), we propose a one-dimensional map, constructed from the standard nontwist map (SNM) [14], a two-dimensional map which locally violates the twist condition [35,36]. For the standard nontwist map defined by [14],

$$y_{n+1} = y_n - b\sin(2\pi x_n),$$
$$x_{n+1} = x_n + a(1 - y_{n+1}^2), \quad \text{mod} \ 1, \qquad (3)$$

where $x \in [0, 1)$, $y \in \mathbb{R}$, and a and b are independent parameters in the range $a \in [0, 1]$ and $b \in \mathbb{R}$ [14].

Repeating the construction for the sine-circle map, but this time using Eqs. (3), we obtain

$$x_{n+1} = x_n + a\{1 - [\Omega - b\sin(2\pi x_n)]^2\}, \qquad (4)$$

where $\Omega = y_n$ and $x \in [0, 1]$. Once the construction is similar to that for the sine-circle map from the standard twist map,

but with the nontwist map, the map in Eq. (4) is called a sine-circle nontwist map.

Expanding the quadratic term in (4), the sine-circle nontwist map can be written as

$$x_{n+1} = x_n + \alpha - \beta \sin(2\pi x_n) + \gamma \cos(4\pi x_n), \quad (5)$$

with $\alpha = a(1 - \Omega^2 - b^2/2)$, $\beta = -2a\Omega b$, and $\gamma = ab^2/2$. Once circle maps are defined as $x_{n+1} = x_n + \Phi + g(x_n)$, with $g(x + 1) = g(x)$ [10,28], the map in (5) is a circle map. In fact, the map is the standard sine-circle map with a harmonic with twice the frequency perturbation. The map with the form presented in (5) can also be obtained from a twist map perturbed by two harmonics of different frequencies, such as

$$I_{n+1} = I_n + \frac{K}{2\pi} \sin(2\pi x_n) + \frac{\Lambda}{2\pi} \cos(4\pi x_n),$$
$$x_{n+1} = x_n + I_{n+1}, \quad (6)$$

with the same mathematical manipulation applied to obtain (2) and (4). It is important to point out that the sine-circle nontwist map is not uniquely connected to the standard nontwist map (3). In fact, twist and nontwist bidimensional maps that present different properties in the two-dimensional space lead to the same one-dimensional circle map. We chose the nomenclature "sine-circle nontwist map" once the SNM was our starting point for this research. Also because of that, we study the map in (4), with the parameters a, b, and Ω, in order to establish a direct relation with the parameters of the SNM.

Following the ranges of a, b, and Ω defined for the SNM, we have $a \in [0, 1]$, $b \in \mathbb{R}$, and $\Omega \in \mathbb{R}$. Once the standard nontwist map is an approximation around $y \approx 0$ [14], we restrict Ω in the range $\Omega \in [-1, 1]$, to be in consonant with Refs. [37–42], which study the map in the range $y \in [-1, 1]$.

Since the first derivative of the map (4) is

$$\frac{dx_{n+1}}{dx_n} = 1 + 4\pi ab[\Omega \cos(2\pi x_n)$$
$$- b \sin(2\pi x_n) \cos(2\pi x_n)], \quad (7)$$

there follows that for a, $b \neq 0$, the map is nonconservative and does not preserve the length ($\frac{dx_{n+1}}{dx_n} \neq 1$) for most parameter values. The map in Eq. (4) is a dissipative one-dimensional map with three control parameters, a, b, and Ω. Because of this, it is not straightforward to find a simple curve in the parameter space where the criticality happens and where the chaotic behavior becomes a possible solution. Therefore it is necessary to apply the known methods to detect the nature of the solutions, such as the Lyapunov exponent and winding number.

The Lyapunov exponent of an orbit (solution) informs us about the mean exponential rate of divergence or convergence of the orbits nearby [28,43,44]. From the sign of the Lyapunov exponent, we have a qualitative view of the dynamics present in the system [43]. For one-dimensional maps, there is only one Lyapunov exponent, and its sign can be positive indicating chaos, negative for periodic orbits, or it can also assume a null value, if the orbit is marginally stable or quasiperiodic [7,43]. For higher-order systems, the number of exponents is equal to the number of degrees of freedom and the dynamics is identified by the analysis of the multiple Lyapunov exponents [43].
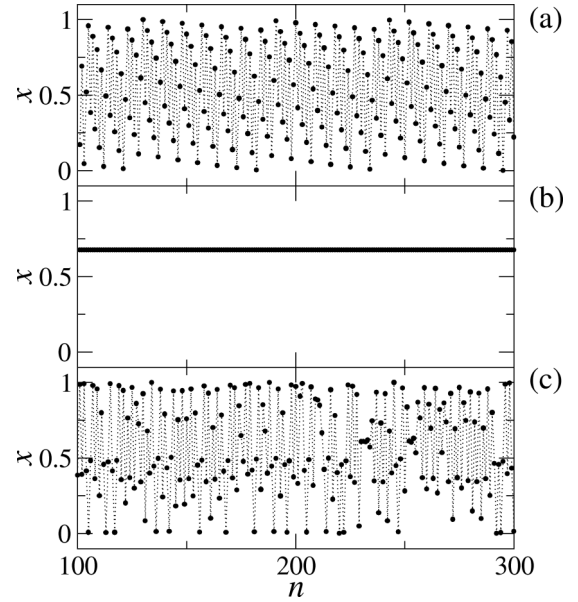

FIG. 1. Time series for the sine-circle nontwist map for (a) $b = 0.15$, (b) $b = 0.56$, and (c) $b = 0.79$. For all series, $x_0 = 0.5$, $a = 0.6$, and $\Omega = 0.5$.

Once our map is one-dimensional, we apply the method for computing the Lyapunov exponent for discrete systems of one dimension. The Lyapunov exponent λ for a one-dimensional map can be determined directly by

$$\lambda = \lim_{T \to \infty} \frac{1}{T} \sum_{n=0}^{T-1} \ln |M'(x_n)|, \quad (8)$$

where M' is the derivative of the map M, i.e., $M' \equiv dM(x)/dx$ [2].

In a first moment, we choose the Lyapunov exponent, calculated by (8), to identify the type of solution the map presents. In order to illustrate the different solutions we can obtain from the map (4), we show three different time series, generated for different values of b, in Fig. 1. We also compute the corresponding Lyapunov exponents for each solution, and their values can be found in Table I.

The three different time series, in Fig. 1, are shown in the range $n \in [100, 300]$ in order to omit the initial transient and to highlight their stationary behavior. For the first series in Fig. 1(a), we observe points distributed in the range $x \in [0, 1]$ that apparently fill the domain and present an organized behavior. For this case we can say we observe a quasiperiodic solution. In the second panel, Fig. 1(b), we observe a periodic solution of period 1. For last series, in Fig. 1(c), we noticed an

TABLE I. Lyapunov exponents (λ) and number of unique recurrence times N_τ for $\epsilon = 0.02$, computed for the time series shown in Fig. 1 for $n = 10^5$ iterations.

	λ	N_τ	Type of solution
(a)	6.343×10^{-6}	3	Quasiperiodic
(b)	-0.104	1	Periodic
(c)	0.625	164	Chaotic

irregular behavior, with points disorganized in the whole domain, suggesting a chaotic solution. We confirm this result by the Lyapunov exponents in Table I. The Lyapunov exponents were calculated by Eq. (8) for a time-series length of $n = 10^5$ iterations. For the quasiperiodic solution, the numerical value for the Lyapunov exponent is $\lambda = 6.343 \times 10^{-6}$, a small numerical value that represents the null value for the exponent. The periodic and chaotic solutions present a negative and positive Lyapunov exponent, respectively.

The winding number provides us the average rotation per iteration and is defined as [28]

$$\omega = \lim_{n \to \infty} \frac{x_n - x_0}{n}, \tag{9}$$

where x_n is the nth iteration of the map for the initial condition x_0. If ω assumes a rational or irrational value, the analyzed solution is periodic or quasiperiodic, respectively. Otherwise, if the limit in Eq. (9) does not converge, the orbit is chaotic. In this study we apply the winding number together with another method, based on the analysis of the recurrence times of an orbit, in order to detect the nature of the solutions. This method is a consequence of Slater's theorem [15,16], which states that for any irrational linear rotation over a unity circle, there are at most three different return times to a connected interval of size $\epsilon < 1$. Moreover, the third return time is the sum of the other two, and two of these three return times are consecutive denominators in the continued fraction expansion of the irrational number, in the interval [0,1]. We can relate Slater's theorem to the quasiperiodic solutions, which rotate according to the irrational winding number ω. Any irrational number γ between 0 and 1 can be expressed uniquely by a continued fraction expansion [28]:

$$\gamma = \frac{1}{a_1 + \frac{1}{a_2 + \frac{1}{a_3 + \cdots}}} \equiv [a_1, a_2, a_3, \ldots]. \tag{10}$$

This expansion is infinite, and if we stop at some element s of the expansion we obtain a convergent $P_s/Q_s = [a_1, a_2, \ldots, a_s]$, which is a rational approximation of the irrational number γ.

To illustrate how Slater's theorem can be applied, we compute the number of unique recurrence times for the parameters and initial condition given in Fig. 1, as well as the winding number for the parameters of Fig. 1(a). We define the center of the recurrence region as the position after the initial transient in order to guarantee that it is on the attractor. In Table I we show the number of unique recurrence N_τ times for the set of parameters of Fig. 1, and we confirm that for the quasiperiodic solution there are only three recurrence times. Moreover, a periodic solution presents only one recurrence time, which is the period itself, and a chaotic solution presents more than three recurrence times.

Since Slater's theorem does not say anything about the size ε of the recurrence region, just that $\epsilon < 1$, for a quasiperiodic solution the values of the recurrence times will change with size ϵ, but the number of them will remain equal to 3. In Table II we show the recurrence times for the quasiperiodic solution with winding number $\omega = 0.442\,441\,495\,099\,428\,43$ for $n = 10^5$ iterations, whose continued fraction expansion is $\omega = [2, 3, 1, 5, 2, 1, 1, 2, 3, 1, 41, 2, 1, 2, 3, \ldots]$, and which

TABLE II. Recurrence times for the quasiperiodic solution, depicted in Fig. 1(a), for different sizes of the recurrence region.

ε	τ
0.020	(9, 43, 52)
0.010	(9,52,61)
0.005	(52,113,165)
0.002	(113,165,278)
0.001	(278,443,721)

has $Q_s = 2, 7, 9, 52, 113, 165, 278, 721, 2441, \ldots$ as the denominators of the convergents P_s/Q_s, for five different sizes of the recurrence region. We see that as ϵ gets smaller, the recurrence times get higher, as expected, and at least two of the three recurrence times are consecutive denominators of the convergents of ω.

In the next section we expand the application of the Lyapunov exponent and the Slater's theorem for different parameter values. Along with bifurcation diagrams, we analyze the nature of the attractors of the map and their evolution with the variation of the control parameters.

III. DYNAMICAL ANALYSIS

In this section we study the nature of the solutions and the evolution of the attractors when the value of a parameter changes. The analysis is based on the computation of the Lyapunov exponent, on the bifurcation diagrams and on the recurrence times using Slater's theorem. Since the map presents three control parameters, we choose to fix the values of Ω and a and to vary the value of b. Fixing $a = 0.1$, we follow the diagrams for $\Omega = 0.5, -0.5$, and $\Omega = 0.0$, with $b \in (0, 2)$. We exclude $b = 0$ because we are interested in the dissipative regime of the map. The result for the bifurcation diagram and the Lyapunov exponent are shown in Fig. 2.

From the bifurcation diagrams shown in Fig. 2, we identify two different attractors. The first type is an attractor that fills the x domain that eventually bifurcates in the second type, the periodic attractor indicated by the distinguishable point(s). This scenario is seen for the three parameters values of Ω. From the Lyapunov exponents values shown in the lower panels of Fig. 2, we observe that a quasiperiodic attractor ($\lambda = 0$) bifurcates and a periodic attractor of period 1 emerges, characterized by a negative Lyapunov exponent. This bifurcation occurs at around $b = 0.5$ for $\Omega = \pm 0.5$ and around $b = 1.0$ for $\Omega = 0.0$. This fixed point attractor eventually suffers a period-doubling bifurcation, and it is replaced by a periodic attractor of period 2, for values of $b > 1.5$ and for the three values of Ω analyzed.

Bifurcations, in one-dimensional maps, occur in the points for which the derivative $\frac{dx_{n+1}}{dx_n}$ has an absolute value equal to unity [2,45]. If $\frac{dx_{n+1}}{dx_n} = 1$, the bifurcation can be a saddle node, pitchfork, or transcritical. On the other hand, a period-doubling bifurcation occurs if $\frac{dx_{n+1}}{dx_n} = -1$ [2,45]. In this paper we focus on the first bifurcation that occurs in the bifurcation diagram, where the quasiperiodic attractor disappears and a fixed point emerges. Therefore the bifurcation point x^* can be
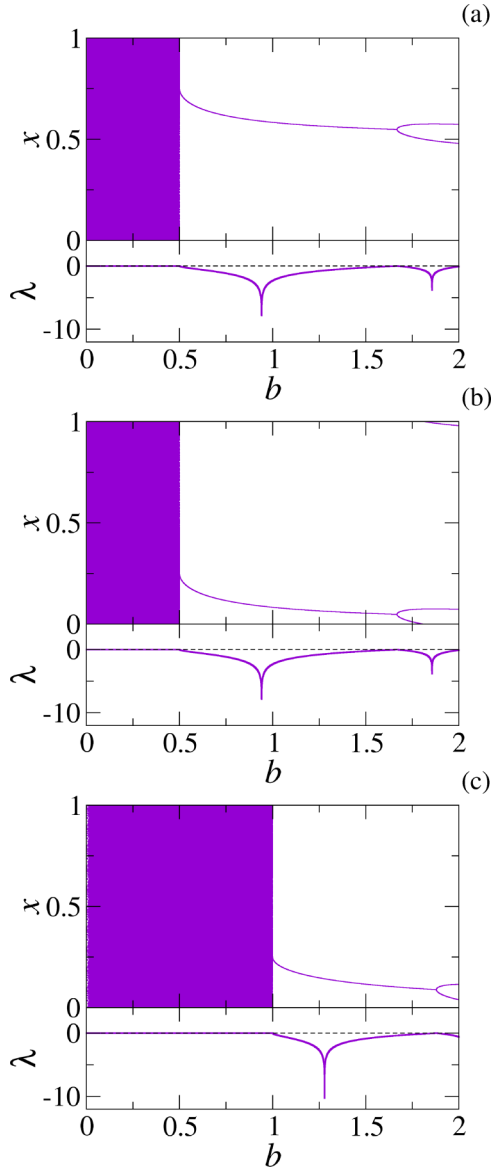
FIG. 2. Bifurcation diagram (top panels) and Lyapunov exponent profile (bottom panels) vs parameter b for $a = 0.1$ and (a) $\Omega = 0.5$, (b) $\Omega = -0.5$, and (c) $\Omega = 0.0$.

calculated by the equation $\frac{\partial x_{n+1}}{\partial x_n}|_{x^*} = 1$, which results in

$$1 + 4\pi ab \cos(2\pi x^*)[\Omega - b \sin(2\pi x^*)] = 1. \quad (11)$$

Equation (11) provides three possible bifurcation points (see the Appendix for calculation details):

$$x_1^* = \frac{1}{4}, \quad x_2^* = \frac{3}{4}, \text{ and } x_3^* = \frac{1}{2\pi} \arcsin\left(\frac{\Omega}{b}\right). \quad (12)$$

Once the bifurcation point corresponds to a fixed point of period 1, the points in (12) must satisfy the relation $x_1^* = x^*$, where x_1^* is the first iteration of the initial condition $x_0 = x^*$. Applying this relation to the fixed points, we obtain the parameter values for which the bifurcation occurs. For x_1^* and x_2^*, the relation $x_1^* = x^*$ is satisfied for $b - \Omega = 1$ and $b + \Omega = 1$, respectively. While for x_3^* the relation is not verified for any

value of a, b, and Ω, x_3^* should be a bifurcation point of higher period. We will not consider in this paper the bifurcation that occurs in x_3^*.

We find two bifurcation curves in the parameter space, $b \pm \Omega = 1$, where the bifurcation occurs at $x = 0.75$ ($x = 0.25$) for the plus (minus) sign, respectively. In fact, in Fig. 2, we see that a bifurcation occurs at $x = 0.75$ for $b = 0.5$ and $\Omega = 0.5$ ($b + \Omega = 1$) and at $x = 0.25$ for $(b, \Omega) = (0.5, -0.5)$ and $(b, \Omega) = (1.0, 0.0)$ ($b - \Omega = 1$).

In order to identify the bifurcation type, we need to compute the derivative with respect to the parameter b, at the bifurcation point. If $\frac{dx_{n+1}}{db} \neq 0$, we have a saddle-node bifurcation, while for $\frac{dx_{n+1}}{db} = 0$ the bifurcation can be a transcritical or pitchfork bifurcation [45]. Since

$$\frac{dx_{n+1}}{db} = 2a \sin(2\pi x_n)[\Omega - b \sin(2\pi x_n)], \quad (13)$$

the derivative is equal to $-2a$, for both bifurcation points x_1^* and x_2^*. Thus the bifurcation curves $b \pm \Omega = 1$ indicate saddle-node bifurcations, for $a \neq 0$. In the bifurcation diagram in Fig. 2, we observe only one bifurcation in the range $b \in (0, 2]$, the bifurcation $b + \Omega = 1$ for $\Omega = 0.5$ and the bifurcation at $b - \Omega = 1$ for $\Omega = -0.5$ and $\Omega = 0.0$.

So far we have analyzed the evolution of the attractors when only one parameter is changed. By continuously varying two parameters and for each set using some method to detect the nature of the solutions, we can construct the parameter space and identify the types of solution and how they are organized. To construct the parameter space for our map, we use the number of recurrence times to identify the solutions. We vary two parameters and keep one fixed, and for each set (a, b, Ω) we iterate the map, with the initial condition $x_0 = 0.5$, for $n = 10^6$, with a transient of 5×10^4, and count the number of unique recurrence times N_τ for a recurrence region of size $\epsilon = 0.02$. If $N_\tau = 1$, the solution is periodic and we plot a black point. The quasiperiodic solution is characterized by three distinct recurrence times, $N_\tau = 3$, and we represented it by a white point. On the other hand, for a chaotic solution we have $N_\tau > 3$ and we plot a red (gray) point. We construct three parameter spaces: (a) $a \times b$, with $\Omega = 0.3$, (b) $\Omega \times a$, with $b = 0.4$, and (c) $\Omega \times b$, with $a = 0.8$. The resulting parameter spaces are shown in Figs. 3(a)–3(c), respectively.

In Fig. 3 we observe a nontrivial structure where the quasiperiodic, periodic, and chaotic regions are intertwined, with shrimp-shaped structures. For low values of a and b, all the solutions are periodic or quasiperiodic. Chaotic solutions start to emerge as these two parameters are increased.

The parameter spaces in Fig. 3 were constructed by the analysis of trajectories, with a single initial condition $x_0 = 0.5$. The results can be significantly different if multistability is present in the system.

IV. MULTISTABILITY

Multistability is the coexistence of different attractors for one set of parameters [46,47]. In this way, various asymptotic behaviors can coexist, and the attractor to which the solution will converge depends strongly on the initial condition [34,46,47]. A comprehensive study about multistability can be found in Ref. [47], where the authors present many systems
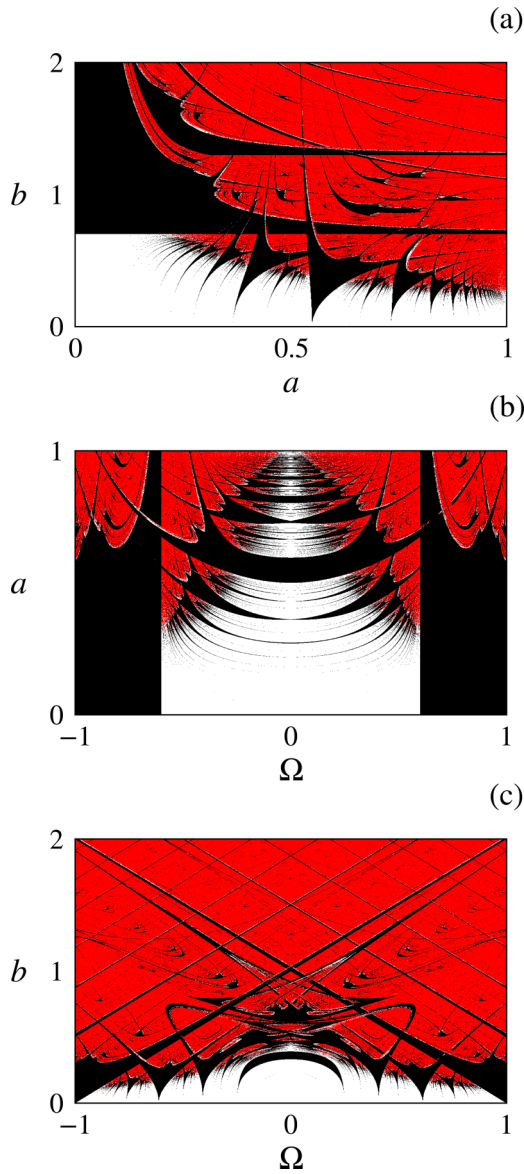
FIG. 3. Parameter spaces for the Slater's condition for (a) $\Omega = 0.3$, (b) $b = 0.4$, and (c) $a = 0.8$. The periodic, quasiperiodic, and chaotic solutions are represented by the black, white, and red (gray) points, respectively.

that present multistable behavior as well as different methods to control it. The multistability in dissipative nontwist systems was study in Ref. [48], and the coexistence of shearless and periodic attractors was observed as the existence of chaotic bands and chaotic attractors on torus. Since the map we are analyzing is derived from the standard nontwist map and it is dissipative, we investigate the possibility of multistable scenarios in this section.

Multistable systems often display hysteresis, i.e., the existence of different evolutions as a parameter is varied in opposite directions. This can be observed, for example, on the bifurcation diagrams. The diagrams in Fig. 2 were constructed by increasing the value of the parameter b. Now we construct and plot two bifurcation diagrams, one increasing the value of b from 0.0 to 2.0 and a second one starting in 2.0 and
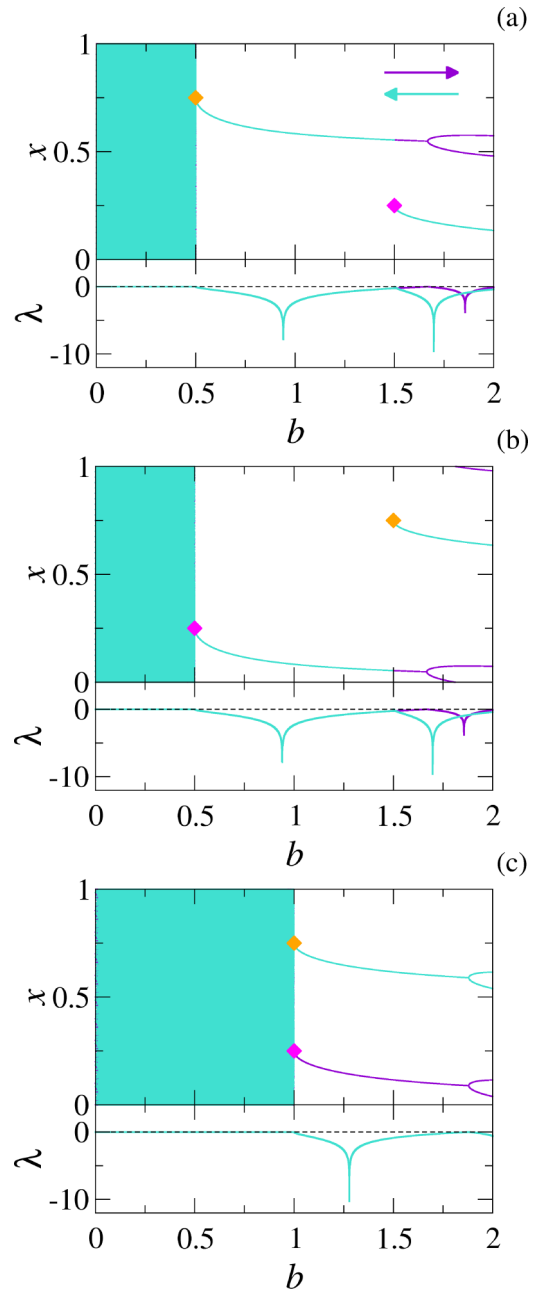

FIG. 4. Bifurcation diagrams and respective Lyapunov exponents vs b for $a = 0.1$, (a) $\Omega = 0.5$, (b) $\Omega = -0.5$, and (c) $\Omega = 0.0$. The purple (dark gray) and turquoise (light gray) points indicate the direction of increasing and decreasing of the parameter, respectively. The direction is also indicated by the colored arrows. The orange (light gray) and pink (dark gray) diamond-shaped points represent the bifurcation that occurs at $b + \Omega = 1$ and $b - \Omega = 1$.

decreasing to 0.0. When computing the diagram in another direction of variation, there is a possibility to follow the evolution of an attractor different from the one analyzed in the first diagram. The results are shown in Fig. 4, along with the corresponding Lyapunov exponents.

In Fig. 4 we observe a distinction between the two overlapping diagrams for $b > 1.5$, when $\Omega = \pm 0.5$, and for $b > 1.0$ at the last case $\Omega = 0.0$. The coexistence of distinguishable turquoise (light gray) and purple (dark gray) points for the

same value of b indicate the coexistence of different attractors in the system. For $\Omega = \pm 0.5$ and $b > 0.5$, the attractor in turquoise is a fixed point of period 1 that suffers an abrupt change in its location, while the purple attractor is also a fixed point but subsequently suffers a period-doubling bifurcation. For $\Omega = 0.0$, both attractors behave in the same way: they are quasiperiodic for $b < 1.0$, and then two fixed points emerge that subsequently bifurcate into a period-2 attractor.

The Lyapunov exponents profiles shown in Fig. 4 provide us the classification of the attractors in the diagram. For the first two cases ($\Omega = \pm 0.5$), it is possible to see the hysteresis also in the Lyapunov exponent profiles for $b > 1.7$. For the case $\Omega = 0.0$, it is impossible to distinguish the two attractors by the Lyapunov exponent profile, but the diagram shows two distinguishable fixed point attractors, representing a scenario of hysteresis in the evolution of the attractor.

We indicate in Fig. 4 the bifurcation points computed in the last section. The bifurcation occurs at $x = 0.75$ for the parameters that satisfied the relation $b + \Omega = 1$, or at $x = 0.25$, when $b - \Omega = 1$ is true. These two cases are indicated by diamond-shape points at the diagrams in Fig. 4, where the orange (pink) point indicates the bifurcation for the case $b + \Omega = 1$ ($b - \Omega = 1$). The bifurcation at $b = 0.5$, for $\Omega = \pm 0.5$, and the two points at $b = 1.0$ for $\Omega = 0.0$, describe the change of the attractor nature: the attractor is quasiperiodic before the bifurcation point and then becomes periodic after it, though the other bifurcation point for $\Omega = \pm 0.5$ ($b = 1.5$) depicts not a change in the behavior but the emergence of other attractor and, consequently, the multistability scenario.

With the last result we can conclude that the bifurcation points are related to the multistability scenario and also the change of the nature of the attractor. In the cases presented in Fig. 4, the multistability is composed by different periodic attractors. However, we cannot affirm that this is always the case for our map. Therefore we now present a method to analyze the possible multistable scenarios for noninvertible, one-dimensional maps.

In order to identify different scenarios of coexistence of attractors for different sets of parameters, we propose a methodology to identify possible attractors scenarios in the map. The method is based in the comparison of the time series resulting from different initial conditions, analysis of the Lyapunov exponents, and the region occupied by the time series in the x domain. If all the initial conditions lead to the same value of the Lyapunov exponent and occupy the same values of x, after some transient time we have a single attractor scenario for the system; otherwise, the multistable scenario is identified. The application of this method is described below.

For a given set of parameters (Ω, a, b), we randomly choose an initial condition $x_0 \in [0, 1]$, evolve it for 5×10^4 iterations, and simultaneously compute its Lyapunov exponent λ. In order to identify if all initial conditions belong to the same basin of attraction and, consequently, all the solutions lead to the same attractor, we analyze different initial conditions and observe if they all assume the same behavior. For this we evolve 100 initial conditions for twice as long, 10^5 iterations, once we are interested in the asymptotic behavior of the solution, and we take the last iteration from x_0, $x_0(n = 5 \times 10^4)$, as a reference to identify periodic solutions. Then

we analyze and compare the x_i values these solutions assume and their Lyapunov exponents λ_{x_i} with the reference values $x_0(n = 5 \times 10^4)$ and λ_{x_0}. With the results of the comparison, we divide the scenarios of the attractors in the system in five classes.

If all the initial conditions lead to the same attractor, we have a scenario of a single attractor in the system. For this scenario to happen, x_0 and all x_i, with $i = 1, 2, ..., 100$, should present a negative Lyapunov exponent and have the same asymptotic behavior. Numerically, we consider this scenario if the reference Lyapunov exponents are smaller than $\lambda_{x_0} = -0.0001$ (periodic solution) and all the solutions generated by the 100 initial conditions return to the reference value $x_0(5 \times 10^4)$, i.e., $|x_i(n) - x_0(5 \times 10^4)| \leqslant 10^{-4}$, for $n > 5 \times 10^4$. With this last condition we ensure the solutions belong to the same attractor.

The single attractor scenario also happens if we have a quasiperiodic attractor in the system. Once the quasiperiodic attractor occupies the entire x domain, in one-dimensional systems, if $\lambda_{x_0} = 0$ (numerically $|\lambda_{x_0}| < 0.0001$), we consider a single attractor scenario composed of a single quasiperiodic attractor. We emphasize that the coexistence of different quasiperiodic attractors is possible [49–51], as well as the coexistence of quasiperiodic and periodic attractors [48] for higher-dimensional maps.

In a multistable scenario composed only by different periodic solutions, we observe that all the Lyapunov exponents are negative, i.e., $\lambda_{x_i} < 0$ for $i = 0, 1, ..., 100$. But in this case, the initial conditions do not belong to the same basin and, consequently, the solutions do not belong to the same attractor. Numerically, if $\lambda_{x_i} < -0.0001$ for all solutions and the condition $|x_i(n) - x_0(5 \times 10^4)| \leqslant 10^{-4}$ is not valid for, at least, one solution x_i, we have a scenario of multistability formed by distinct periodic solutions.

We consider a multistable scenario formed by chaotic and periodic attractors if at least one periodic and one chaotic solution is identified. For this we analyze all 101 solutions, the reference initial condition plus the others 100 randomly chosen, and observe their Lyapunov exponents. If at least one is negative and one is positive ($\lambda_{x_i} > 0.0001$), the coexistence between chaotic and periodic attractors is confirmed. In most cases the chaotic attractor appears in the form of chaotic bands occupying a defined region in the x domain.

The fourth class we define is related to the chaotic behavior in the system. In this class all the initial conditions generate a chaotic solution and belong to the same chaotic attractor. In order to identify this situation, we compute the Lyapunov exponent of all the solutions and verify if all are positive. If this is the case, we then analyze whether all of them belong to the same attractor, i.e., if there is not a coexistence of chaotic bands. We consider that all solutions are in the same chaotic behavior if they occupy the same region in the x domain. For this we compare the time average of the last 5×10^4 iterates of all solutions. In our simulations, the attractor is unique if the average is smaller than 0.1, $|\bar{x}_i - \bar{x}_1| < 0.1$, for all $i = 2, 3, ..., 100$. The time averages are computed as $\bar{x}_i = \frac{1}{n_0 - n_1} \sum_{n=n_0}^{n_1} x_i(n)$, where $n_0 = 5 \times 10^4$ and $n_1 = 10^5$. The reference solution, x_0, must be chaotic as well ($\lambda_{x_0} > 0$).

The last class is related to the coexistence of chaotic bands, chaotic behaviors restricted to a certain region of the

x domain. The procedure is the same as that proposed in the last case (chaos scenario), but the condition $|\bar{x}_i - \bar{x}_1| < 0.1$ should not be valid for at least one initial condition. If this is the case, we have a multistable scenario composed by multiple chaotic bands. The value 0.1 used for the condition is chosen based on our computations of the averages $\bar{x}_i$ for cases with different chaotic bands.

We perform the analysis described above for different sets of parameters (Ω, a, b) and we constructed three parameter spaces: (a) $a \times b$ for $\Omega = 0.3$, (b) $\Omega \times a$ for $b = 0.4$, and (c) $\Omega \times b$ for $a = 0.8$, the same parameter values in Figs. 3(a)–3(c). Each scenario is identified by a different color, and the results are shown in Fig. 5, providing us the multistable scenario for different parameters sets (a, b, Ω).

The blue points indicate parameters where the single attractor scenario is present. The only attractor can be periodic or quasiperiodic. These situations are dominant in the parameter space for $\Omega = 0.3$ [Fig. 5(a)] and $b = 0.4$ [Fig. 5(b)]. When the system presents only chaotic behavior, in which all the solutions occupy chaotically the same range of x, we have the chaotic scenario, depicted by the green points. The multistable scenarios are represented by the red, yellow, and black points, which indicate the coexistence of periodic attractors, periodic and chaotic attractors, and chaotic bands, respectively. These scenarios occupy a smaller region in the parameter space when compared to those occupied by the blue and green points (single attractor and chaotic scenario), and they can be found mostly after the bifurcation lines (orange and pink lines), i.e., for slightly greater values, when we follow the increase of the parameter.

The scenarios of multistability located after the bifurcation lines are in accordance with the result shown in Fig. 3, where the coexistence of attractor can emerge at the bifurcation point. However, this is not a rule once we can observe multistable scenarios, mostly indicated by red points (coexistence of different periodic attractors) for parameter values smaller than those at the bifurcation curves, in all panels of Fig. 5. The chaotic regime is predominant for larger parameter values, but since the system depends on three parameters, we are unable to define exactly when the emergence of chaotic behavior occurs, so it is necessary to perform the analysis for each set (Ω, a, b).

From the parameter spaces depicted in Fig. 5, we conclude that it is possible to identify scenarios of multistability or single attractors, but we cannot predict the particular scenario for a specific set of parameters. The structure of the parameter space is nontrivial, and there are not smooth or simple boundaries between the different scenarios. Instead, the boundaries are complex and can even be fractal, due to the similarity of some parts of the blue region with the Arnold tongues [28] and phase-locking scenarios in parameter spaces, for example, Fig. 2 in Ref. [52].

For the construction of Fig. 5, we consider the possibility of the existence of chaotic bands, defined by the chaotic behavior that occurs in a restricted region of the x domain. We also observe chaotic attractors in the system that fill the entire range of x. Knowing that different chaotic structures exist in the system, we now analyze how they evolve with the change of the parameters and if a crisis can be observed in the system.
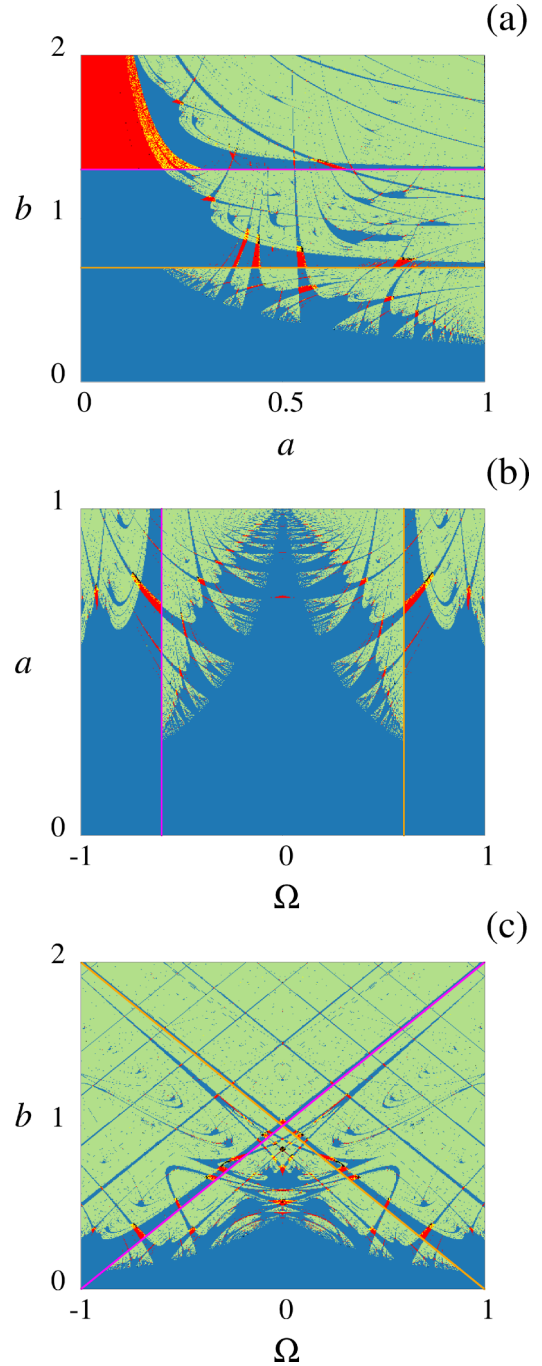

FIG. 5. Parameter spaces for the multistable scenarios of the system for (a) $\Omega = 0.3$, (b) $b = 0.4$, and (c) $a = 0.8$. The single attractor scenario, the multistable scenarios as the coexistence of periodic attractors, periodic and chaotic attractors and distinct chaotic bands, and the chaotic behavior are represented by blue (dark gray), red (gray), yellow (white), and black and green (light gray) points, respectively. The bifurcation curves $b + \Omega = 1$ and $b - \Omega = 1$ are shown as the orange (light gray) and pink (gray) lines.

A crisis can be defined as an event where the chaotic attractor changes discontinuously when an unstable periodic orbit collides with the chaotic attractor [53]. The attractor after crisis can have its size abruptly increased or it can be extinct, becoming a chaotic transient. For the first case, the
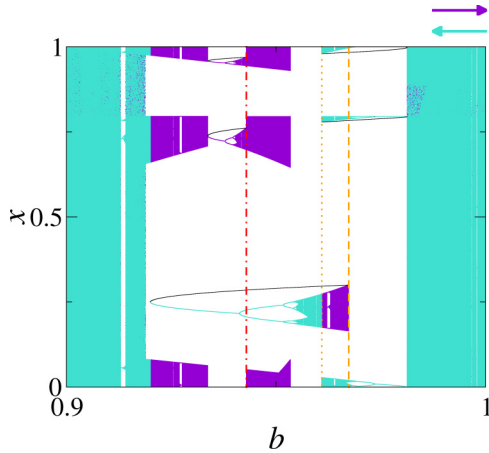
FIG. 6. Bifurcation diagrams vs the parameter b for $a = 0.8$, $\Omega = -0.08$. The purple (dark gray) and turquoise (light gray) points indicate the increasing (decreasing) direction of the parameter b, respectively. The black solid curves represent the unstable periodic orbits. The dash-dotted red (dark gray) line indicates the interior crisis at $b \approx 0.9429$, while the orange (gray) lines mark the boundary crisis at $b \approx 0.9609$ (dotted line) and $b \approx 0.9673$ (dashed line).

unstable periodic orbit collides within the basin of attraction, the crisis is named as an interior crisis, and the attractor grows in size [53]. The second case, the attractor and its basin, disappears by the collision of the unstable periodic orbit with the boundary of the basin, thus having a boundary crisis [53].

In order to investigate the scenarios of crisis in our one-dimensional map defined by Eq. (4), we constructed the bifurcation diagram for $a = 0.8$ and $\Omega = -0.08$, varying the value of b in the range $b \in [0.9, 1]$. As we performed in Fig. 4, we also compute the diagram for the increase and the decrease of the parameter b. The diagram is shown in Fig. 6.

We observe hysteresis in the ranges $b \in [0.92, 0.955]$ and $b \in [0.961, 0.967]$, in which the purple and the turquoise points are distinguishable, indicating more than one attractor for the same set of parameters. The multistability scenario in these ranges is formed by the coexistence between periodic and chaotic bands, different periodic attractors, and also between different chaotic bands (second range).

The chaotic bands undergo abrupt changes as the value of b varies. First we observe an abrupt expansion in the attractor, around $b \approx 0.943$. We also observe, for $b \approx 0.967$, the extinction of the purple chaotic band, and for $b \approx 0.961$, the extinction of the turquoise chaotic bands. These results suggest that the chaotic attractors passes through an interior crisis and a boundary crisis, respectively. In order to confirm the existence of the crises, we plot the unstable periodic orbits together with the diagram, indicated by the solid black curves. The unstable orbits are obtained for the following procedure. After we assume the period T of these orbits, we ran the domain $x \in [0, 1]$ and we compute the difference $|x_T - x_0|$, where x_0 is the initial condition we are analyzing. Once the orbits are unstable, they diverge from the initial condition quickly, if they are not really close to the fixed point. Therefore we define that if $|x_T - x_0| < 10^{-6}$, the x_0 belong to the periodic orbits. In order to identify if the orbit is unstable or stable, we compute the derivative at the point. If it is greater

than unity, the orbit is unstable. We also analyze orbits generated by the initial condition nearby, x_0. If they diverge and are attracted to other fixed points, we assume x_0 is unstable. With this procedure we computed the unstable periodic points in Fig. 6, where we can observe unstable periodic orbits of period 1 and period 2.

We can identify the two types of crises in the bifurcation diagram of Fig. 6. The period-2 unstable periodic orbit collides with the purple chaotic bands, and an abrupt increase of the attractor emerges after the collision, an interior crisis (dash-dotted red line). The boundary crisis is observed with the collision between the unstable periodic orbit of period 1 with the purple chaotic band (dashed orange line), followed by the extinction of the chaotic attractor. We assume that the unstable periodic orbit belongs in the basin boundary, for a boundary crisis, reminding us that the attractor collides with its own basin boundary. A similar scenario occurs when the period-2 unstable periodic orbit collides with the turquoise chaotic bands (dotted orange line), after which the chaotic attractor is extinct.

The extinction of the attractors by the boundary crisis plays an important role with regard to the multistability scenario. If we observe the direction of increasing the parameter b, the boundary crisis occurs at $b = 0.9673$, and the purple band is destroyed along with multistability. If we follow the opposite direction, the boundary crisis occurs at $b = 0.9609$, the turquoise bands are extinct, and a scenario of a single attractor emerges, until $b \approx 0.953$, where purple chaotic bands arise in the bifurcation diagram.

V. CONCLUSIONS

We proposed a one-dimensional circle map that exhibits a three-parameter dependency. The map can be constructed from the manipulation of two different two-dimensional maps: the standard nontwist map and a twist map perturbed by two harmonics with different frequencies. From our simulations of the Lyapunov exponent and the application of Slater's theorem, we were able to identify the different solutions of the systems—the periodic, quasiperiodic, and chaotic behavior. We present this map as a one-dimensional system that can be interpreted as a local approximation of the standard nontwist map when the respective y is constant.

From the analytical and numerical studies on the bifurcations displayed by the map, we were able to identify two bifurcation curves in the parameter space, $b \pm \Omega = 1$, for which the bifurcation that occurs is of the saddle-node type. This point is also indicative for the onset of multistability. These shifts from a single attractor to multistable scenario, passing through the bifurcation, only occur when different single attractor tongues intercept each other.

In order to identify the nature of the map solutions, we applied Slater's theorem as an alternative to the Lyapunov exponent. We observed three possible distinct solutions: the periodic solution, with one return time; the quasiperiodic solution, with three different return times; and the chaotic behavior, with more than three return times. With the application of the condition asserted by Slater [15,16], the numerical thresholds for the negative, null, and positive Lyapunov exponents are not necessary conditions.

Multistability is a possible scenario for our one-dimensional model. The coexistence of different periodic attractors was observed by the hysteresis of the bifurcation diagram. The two bifurcation points, obtained by the lines $b \pm \Omega = 1$, correspond to two different attractors that coexist for the same parameters (Ω, a, b). In order to broaden the identification of multistable scenarios for different parameters values, we proposed a method based on the comparison between the Lyapunov exponent and the region occupied in the x domain related to the solutions obtained by the iteration of distinct initial conditions. From our simulations we observed the prevalence of single attractor and chaotic scenarios, and we analyze the multistable scenarios for the three parameter spaces. The multistable scenarios are restricted to smaller regions of the space, and its majority is composed of the coexistence of different periodic attractors, while the points which indicate the coexistence of chaotic and periodic attractors and distinct chaotic bands are minority.

Finally, we analyzed the crisis involving the chaotic attractors of the map: the interior crisis, responsible for the abrupt increase in the size of the chaotic attractor, and the boundary crisis, accountable for the extinction of the attractors and which occurs twice in the diagram. While the interior crisis does not affect the multistability, the boundary crises are responsible for the extinction of the multistable scenario. Following the diagram in the direction of increasing parameter b, we observe that the crisis indicates the extinction of a chaotic band and also the end of multistability. If we follow the diagram in the opposite direction, decreasing the value of b, the boundary crisis also indicated the extinction of chaotic bands and the end of the multistable scenario.

The study presented in this paper has, as a novelty, the detailed analysis of bifurcation and multistability for a one-dimensional map with a three-parameter dependency. We also applied the Slater's theorem, an effective method to identify the nature of the solutions that are not used as much in the literature. Slater's theorem is useful once it is not necessary to establish a numerical threshold for the positive, negative, and null values of the Lyapunov exponent to identify the nature of the attractors. We hope that further studies on the map will shed light on other issues that were not analyzed in this paper, such as basins of attraction, the fractability of parameter spaces, and topological chaos, among other questions. We also expect that other methodologies, such as the rotation intervals [19,54], will bring interesting results for the dynamical analysis of the map.

APPENDIX: BIFURCATION ANALYSIS

The saddle-node bifurcation occurs in one-dimensional maps when $\partial x_{n+1}/\partial x_n|_{(x^*, \alpha^*)} = 1$ and $\partial x_{n+1}/\partial \alpha|_{(x^*, \alpha^*)} \neq 0$, where α is the control parameter [45]. In order to prove the bifurcation visualized in Figs. 2 and 4 are saddle-node bifurcations, we show the calculation of the derivatives $\partial x_{n+1}/\partial x_n$ and $\partial x_{n+1}/\partial b$.

Once we are not considering the period-doubling bifurcation ($\partial x_{n+1}/\partial x_n = -1$), the derivative $\partial x_{n+1}/\partial x_n$ must be equal to unity:

$$\left.\frac{\partial x_{n+1}}{\partial x_n}\right|_{x^*} = 1,$$

$$1 + 4\pi ab \cos(2\pi x^*)[\Omega - b\sin(2\pi x^*)] = 1,$$

$$4\pi ab \cos(2\pi x^*)[\Omega - b\sin(2\pi x^*)] = 0,$$

$$\cos(2\pi x^*)[\Omega - b\sin(2\pi x^*)] = 0.$$

Hence we obtain the following conditions:

$$\begin{cases} \cos 2\pi x^* = 0 \begin{cases} 2\pi x^* = \frac{\pi}{2} \rightarrow x^* = \frac{1}{4}, \\ 2\pi x^* = \frac{3\pi}{2} \rightarrow x^* = \frac{3}{4}, \end{cases} \\ \Omega - b\sin(2\pi x^*) = 0 \rightarrow x^* = \frac{1}{2\pi}\arcsin\left(\frac{\Omega}{b}\right). \end{cases} \quad \text{(A1)}$$

Once we analyze the bifurcation in fixed points of period 1, the next iterate x_{n+1} must be identical to x_n, with $x_n = x^*$. Therefore $x_{n+1}(x_n = x^*) = x^*$, and

$$x^* = x^* + a[1 - (\Omega - b\sin(2\pi x^*))]^2,$$

$$b\sin(2\pi x^*) = \Omega \pm 1. \quad \text{(A2)}$$

Entering the points from Eq. (12) in (A2), we obtain, for $x^* = \frac{1}{4}$,

$$b\sin\left(2\pi\frac{1}{4}\right) = \Omega \pm 1, \quad \text{(A3)}$$

$$b - \Omega = \pm 1,$$

while for $x^* = \frac{3}{4}$,

$$b\sin\left(2\pi\frac{3}{4}\right) = \Omega \pm 1,$$

$$b + \Omega = \pm 1. \quad \text{(A4)}$$

Lastly, for $x^* = \frac{1}{2\pi}\arcsin(\frac{\Omega}{b})$, we obtain the relation $\Omega = \Omega \pm 1$, and there is not a value of Ω that satisfies the equality. As $b > 0$ and $-1 \leqslant \Omega \leqslant 1$, the bifurcation at $x^* = 1/4$ ($x^* = 3/4$) occurs when $b - \Omega = 1$ ($b + \Omega = 1$).

Computing the derivative $\partial x_{n+1}/\partial b$, we obtain

$$\frac{\partial x_{n+1}}{\partial b} = 2a\sin(2\pi x_n)[\Omega - b\sin(2\pi x_n)]. \quad \text{(A5)}$$

At the bifurcation points ($x^* = 1/4, \Omega^*, b^* - \Omega^* = 1$) and ($x^* = 3/4, \Omega^*, b^* + \Omega^* = 1$), for both points the derivative assumes the value

$$\left.\frac{\partial x_{n+1}}{\partial b}\right|_{(x^*, \Omega^*, b^*)} = -2a, \quad \text{(A6)}$$

which is not null for $a \neq 0$.

[1] R. M. May, Simple mathematical models with very complicated dynamics, Nature (London) **261**, 459 (1976).

[2] E. Ott, *Chaos in Dynamical Systems* (Cambridge University Press, Cambridge, England, 2002).

[3] R. L. Viana and F. F. d. Carvalho, Sincronização entre um oscilador de fase e um forçamento externo, Revista Brasileira de Ensino de Física **39**, e3306 (2017).

[4] P. Bak, T. Bohr, and M. H. Jensen, Mode-locking and the transition to chaos in dissipative systems, Phys. Scr. **1985**, 50 (1985).

[5] A. Csordas, G. Györgyi, P. Szepfalusy, and T. Tel, Statistical properties of chaos demonstrated in a class of one-dimensional maps, Chaos: An Interdisciplinary Journal of Nonlinear Science **3**, 31 (1993).

[6] V. I. Arnol'd, Small denominators. I. On the mappings of the circle on itself, Izvestiya Rossiiskoi Akademii Nauk. Seriya Matematicheskaya **25**, 21 (1961).

[7] U. Feudel, J. Kurths, and A. S. Pikovsky, Strange non-chaotic attractor in a quasiperiodically forced circle map, Physica D **88**, 176 (1995).

[8] O. Afsar and U. Tirnakli, Probability densities for the sums of iterates of the sine-circle map in the vicinity of the quasiperiodic edge of chaos, Phys. Rev. E **82**, 046210 (2010).

[9] D. J. Olinger, A. B. Chhabra, and K. R. Sreenivasan, The onset of chaos in the wake of an oscillating cylinder: Experiment and the dynamics of the circle map, Pramana **48**, 693 (1997).

[10] T. Bohr, P. Bak, and M. H. Jensen, Transition to chaos by interaction of resonances in dissipative systems. II. Josephson junctions, charge-density waves, and standard maps, Phys. Rev. A **30**, 1970 (1984).

[11] M. J. Feigenbaum, L. P. Kadanoff, and S. J. Shenker, Quasiperiodicity in dissipative systems: A renormalization group analysis, Physica D **5**, 370 (1982).

[12] S.-Y. Kim and D.-S. Lee, Transition to chaos in a dissipative standardlike map, Phys. Rev. A **45**, 5480 (1992).

[13] E. W. Weisstein, Circle map, From MathWorld–A Wolfram Web Resource, https://mathworld.wolfram.com/CircleMap.html.

[14] D. del Castillo-Negrete and P. J. Morrison, Chaotic transport by Rossby waves in shear flow, Phys. Fluids **5**, 948 (1993).

[15] N. B. Slater, The distribution of the integers n for which $\theta n < \varphi$, Math. Proc. Cambridge Philos. Soc. **46**, 525 (1950).

[16] N. B. Slater, Gaps and steps for the sequence nθ mod 1, Math. Proc. Cambridge Philos. Soc. **63**, 1115 (1967).

[17] E. G. Altmann, G. Cristadoro, and D. Pazó, Nontwist non-Hamiltonian systems, Phys. Rev. E **73**, 056201 (2006).

[18] Y. Zou, D. Pazó, M. C. Romano, M. Thiel, and J. Kurths, Distinguishing quasiperiodic dynamics from chaos in short-time series, Phys. Rev. E **76**, 016210 (2007).

[19] R. S. Mackay and C. Tresser, Transition to topological chaos for circle maps, Physica D **19**, 206 (1986).

[20] J. A. C. Gallas, Dissecting shrimps: Results for some one-dimensional physical models, Physica A **202**, 196 (1994).

[21] J. A. C. Gallas, Structure of the Parameter Space of the Hénon Map, Phys. Rev. Lett. **70**, 2714 (1993).

[22] A. Hoff, D. T. da Silva, C. Manchein, and H. A. Albuquerque, Bifurcation structures and transient chaos in a four-dimensional Chua model, Phys. Lett. A **378**, 171 (2014).

[23] S. L. T. de Souza, A. A. Lima, I. L. Caldas, R. O. Medrano-T., and Z. O. Guimarães-Filho, Self-similarities of periodic structures for a discrete model of a two-gene system, Phys. Lett. A **376**, 1290 (2012).

[24] E. S. Medeiros, S. L. T. de Souza, R. O. Medrano-T, and I. L. Caldas, Periodic window arising in the parameter space of an impact oscillator, Phys. Lett. A **374**, 2628 (2010).

[25] V. dos Santos, J. D. Szezech Jr., M. S. Baptista, A. M. Batista, and I. L. Caldas, Unstable dimension variability structure in the parameter space of coupled hénon maps, Appl. Math. Comput. **286**, 23 (2016).

[26] G. M. Zaslavsky, *Hamiltonian Chaos and Fractional Dynamics* (Oxford University Press on Demand, 2005).

[27] J. S. E. Portela, I. L. Caldas, and R. L. Viana, Tokamak magnetic field lines described by simple maps, Eur. Phys. J.: Spec. Top. **165**, 195 (2008).

[28] A. J. Lichtenberg and M. A. Lieberman, *Regular and Chaotic Dynamics* (Springer Science & Business Media, 2013), Vol. 38.

[29] Z. Chen and S. W. Pan, Study of phase circle map model and its symbolic dynamics, in *2015 International Conference on Electrical, Automation and Mechanical Engineering* (Atlantis Press, Amsterdam, 2015), pp. 729–733.

[30] U. Tırnaklı, C. Tsallis, and M. L. Lyra, Circular-like maps: Sensitivity to the initial conditions, multifractality and nonextensivity, Eur. Phys. J. B **11**, 309 (1999).

[31] J. H. E. Cartwright, Newton maps: Fractals from Newton's method for the circle map, Comput. Graphics **23**, 607 (1999).

[32] J. C. B. de Figueiredo and C. P. Malta, Lyapunov graph for two-parameters map: Application to the circle map, Int. J. Bifurcation Chaos **08**, 281 (1998).

[33] P. Cvitanovic, B. Shraiman, and B. Söderberg, Scaling laws for mode lockings in circle maps, Phys. Scr. **32**, 263 (1985).

[34] U. Feudel and C. Grebogi, Multistability and the control of complexity, Chaos: An Interdisciplinary Journal of Nonlinear Science **7**, 597 (1997).

[35] D. del Castillo-Negrete, J. M. Greene, and P. J. Morrison, Area preserving nontwist maps: Periodic orbits and transition to chaos, Physica D **91**, 1 (1996).

[36] K. Fuchss, A. Wurm, A. Apte, and P. J. Morrison, Breakup of shearless meanders and "outer" tori in the standard nontwist map, Chaos: An Interdisciplinary Journal of Nonlinear Science **16**, 033120 (2006).

[37] M. Mugnaine, A. C. Mathias, M. S. Santos, A. M. Batista, J. D. Szezech Jr., and R. L. Viana, Dynamical characterization of transport barriers in nontwist Hamiltonian systems, Phys. Rev. E **97**, 012214 (2018).

[38] J. D. Szezech Jr., I. L. Caldas, S. R. Lopes, P. J. Morrison, and R. L. Viana, Effective transport barriers in nontwist systems, Phys. Rev. E **86**, 036206 (2012).

[39] I. L. Caldas, R. L. Viana, C. V. Abud, J. C. D. d. Fonseca, Z. d. O. Guimarães Filho, T. Kroetz, F. A. Marcus, A. B. Schelin, J. Szezech, D. L. Toufen *et al.*, Shearless transport barriers in magnetically confined plasmas, Plasma Phys. Controlled Fusion **54**, 124035 (2012).

[40] A. C. Mathias, M. Mugnaine, M. S. Santos, J. D. Szezech Jr., I. L. Caldas, and R. L. Viana, Fractal structures in the parameter space of nontwist area-preserving maps, Phys. Rev. E **100**, 052207 (2019).

[41] M. S. Santos, M. Mugnaine, J. D. Szezech Jr., A. M. Batista, I. L. Caldas, M. S. Baptista, and R. L. Viana, Recurrence-based analysis of barrier breakup in the standard nontwist map,

Chaos: An Interdisciplinary Journal of Nonlinear Science **28**, 085717 (2018).

[42] J. D. Szezech Jr., I. L. Caldas, S. R. Lopes, R. L. Viana, and P. J. Morrison, Transport properties in nontwist area-preserving maps, Chaos: An Interdisciplinary Journal of Nonlinear Science **19**, 043108 (2009).

[43] A. Wolf, J. B. Swift, H. L. Swinney, and J. A. Vastano, Determining Lyapunov exponents from a time series, Physica D **16**, 285 (1985).

[44] G. Benettin, L. Galgani, A. Giorgilli, and J.-M. Strelcyn, Lyapunov characteristic exponents for smooth dynamical systems and for Hamiltonian systems; A method for computing all of them. Part 1: Theory, Meccanica **15**, 9 (1980).

[45] K. T. Alligood, T. D. Sauer, and J. A. Yorke, *Chaos* (Springer, New York, 1996).

[46] U. Feudel and C. Grebogi, Why Are Chaotic Attractors Rare in Multistable Systems? Phys. Rev. Lett. **91**, 134102 (2003).

[47] A. N. Pisarchik and U. Feudel, Control of multistability, Phys. Rep. **540**, 167 (2014).

[48] M. Mugnaine, A. M. Batista, I. L. Caldas, J. D. Szezech, R. E. de Carvalho, and R. L. Viana, Curry-Yorke route to shearless attractors and coexistence of attractors in dissipative nontwist systems, Chaos: An Interdisciplinary Journal of Nonlinear Science **31**, 023125 (2021).

[49] G. Li, Y. Yue, C. Grebogi, D. Li, and J. Xie, Strange nonchaotic attractors and multistability in a two-degree-of-freedom quasiperiodically forced vibro-impact system, Fractals **29**, 2150103 (2021).

[50] J. P. Singh, J. Koley, K. Lochan, and B. K. Roy, Presence of megastability and infinitely many equilibria in a periodically and quasi-periodically excited single-link manipulator, Int. J. Bifurcation Chaos **31**, 2130005 (2021).

[51] P. Prakash, K. Rajagopal, J. P. Singh, and B. K. Roy, Megastability in a quasi-periodically forced system exhibiting multistability, quasi-periodic behaviour, and its analogue circuit simulation, AEU Int. J. Electron. Commun. **92**, 111 (2018).

[52] R. Perez and L. Glass, Bistability, period doubling bifurcations and chaos in a periodically forced oscillator, Phys. Lett. A **90**, 441 (1982).

[53] C. Grebogi, E. Ott, and J. A. Yorke, Chaotic Attractors in Crisis, Phys. Rev. Lett. **48**, 1507 (1982).

[54] R. MacKay, Rotation interval from a time series, J. Phys. A: Math. Gen. **20**, 587 (1987).